

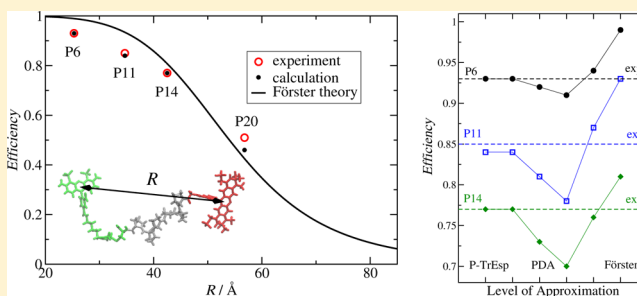
Theory of FRET “Spectroscopic Ruler” for Short Distances: Application to Polyproline

Ekaterina Sobakinskaya, Marcel Schmidt am Busch, and Thomas Renger*[✉]

Institut für Theoretische Physik, Johannes Kepler Universität Linz, Altenberger Str. 69, 4040 Linz, Austria

Supporting Information

ABSTRACT: Förster resonance energy transfer (FRET) is an important mechanism for the estimation of intermolecular distances, e.g., in fluorescent labeled proteins. The interpretations of FRET experiments with standard Förster theory relies on the following approximations: (i) a point-dipole approximation (PDA) for the coupling between transition densities of the chromophores, (ii) a screening of this coupling by the inverse optical dielectric constant of the medium, and (iii) the assumption of fast isotropic sampling over the mutual orientations of the chromophores. These approximations become critical, in particular, at short intermolecular distances, where the PDA and the screening model become invalid and the variation of interchromophore distances, and not just orientations, has a critical influence on the excitation energy transfer. Here, we present a quantum chemical/electrostatic/molecular dynamics (MD) method that goes beyond all of the above approximations. The Poisson-TrEsp method for the ab initio/electrostatic calculation of excitonic couplings in a dielectric medium is combined with all-atom molecular dynamics (MD) simulations to calculate FRET efficiencies. The method is applied to analyze single-molecule experiments on a polyproline helix of variable length labeled with Alexa dyes. Our method provides a quantitative explanation of the overestimation of FRET efficiencies by the standard Förster theory for short interchromophore distances for this system. A detailed analysis of the different levels of approximation that connect the present Poisson-TrEsp/MD method with Förster theory reveals error compensation effects, between the PDA and the neglect of correlations in interchromophore distances and orientations on one hand and the neglect of static disorder in orientations and interchromophore distances on the other. Whereas the first two approximations are found to decrease the FRET efficiency, the latter two overcompensate this decrease and are responsible for the overestimation of the FRET efficiency by Förster theory.



INTRODUCTION

Förster resonance energy transfer (FRET), introduced in the late 1940s of the last century,¹ has become one of the most important methods to measure distances in macromolecules, since its introduction as a “spectroscopic ruler” in 1967 by Stryer and Haugland.² Over recent years, there has been substantial interest in the application of the single-molecule FRET technique to studying biomolecules^{3–9} that triggered the development of advanced analysis tools.^{4,10–13} In the experiment, FRET is measured between a donor and an acceptor chromophore, which are attached to the biomolecule. A nonradiative relaxation process transmits the electronic excitation from the initially excited donor to the acceptor chromophore, which is initially in the ground state. The efficiency of the transfer depends on the distance between the chromophores as well as on their mutual orientation. In the experiment, the transfer efficiency is determined via the measured fluorescence intensity of the donor, I_D , and acceptor, I_A , as¹⁴

$$E = \frac{I_A}{I_A + \gamma I_D} \quad (1)$$

where $\gamma = \phi_A \sigma_A / (\phi_D \sigma_D)$ takes into account differences in the fluorescence quantum yield ϕ and the sensitivity σ of the detector for the photons of the donor (D) and the acceptor (A). From Förster theory for excitation energy transfer, the well-known simple expression for the FRET efficiency is²

$$E(R) = \frac{1}{1 + \left(\frac{R}{R_0}\right)^6} \quad (2)$$

where R is the center-to-center distance between the chromophores and the Förster radius R_0 is defined via¹

$$R_0^6 = \frac{9000(\ln 10)\phi_D O_{al} 2}{128\pi^5 N_A n^4 3} \quad (3)$$

containing the fluorescence quantum yield of the donor ϕ_D , the overlap integral $O_{al} = \int_0^\infty d\nu \alpha_A(\nu) I_D(\nu) / \nu^4$ of the experimental absorption spectrum $\alpha_A(\nu)$ of the acceptor (in molar

Received: September 26, 2017

Revised: November 27, 2017

Published: November 30, 2017

absorbance) and the area-normalized emission spectrum $I_D(\nu)$ of the donor, N_A is Avogadro's constant, and n is the refractive index of the medium. As seen in eq 2, the Förster radius R_0 denotes the distance at which $E = 0.5$, that is, 50% of the donor excitation is transferred to the acceptor and 50% decays to the ground state of the donor. The independent determination of the different quantities entering the Förster radius R_0 from spectroscopy on the isolated chromophores is of great practical use because it allows the interchromophore distance R to be predicted using eq 2

$$R(E) = R_0(E^{-1} - 1)^{1/6} \quad (4)$$

in the coupled system from measured FRET efficiencies E , without free parameters. However, the simplicity of the expression is only obtained after applying several considerable approximations. Central to the formulation is the assumption that the transition densities of the donor and the acceptor interact as point transition dipoles, where the screening of this Coulomb interaction is described as $1/n^2$, with n being the refractive index of the environment. In addition, the chromophores are assumed to rotate "freely" in the average of the square of the coupling matrix element over mutual pigment orientations giving rise to the factor $2/3$ in R_0^6 in eq 3. Despite the general success of Förster theory, there are cases where some of the approximations become invalid and the theory needs to be extended, as has been reviewed, e.g., in refs 15–17.

As noted above, at close interchromophore distances, one expects the point-dipole approximation (PDA) to fail because the chromophores experience more details of the other chromophore's transition density. The validity of the PDA has been investigated by quantum chemical methods,^{18–20,22–26} as the transition density cube method¹⁸ allowing for a numerically exact calculation of the Coulomb coupling. Application of these methods enabled estimation of the PDA accuracy for different systems. For bacteriochlorophyll *a* (BChl *a*) pigments, the PDA was reported to work reasonably well for center-to-center separations >15 Å.¹⁸ For the B850 ring of strongly coupled BChl *a* pigments, with center-to-center distances <10 Å, in the light-harvesting complex LH2 of purple bacteria, the PDA significantly overestimates the excitonic couplings.¹⁹ A qualitatively similar but even more dramatic effect was reported²² for the excitonic coupling between a segment of polyfluorene (PF₆) and tetraphenylporphyrin (TPP) using semiempirical quantum chemical calculations. In this study, the PDA was found to overestimate the excitonic coupling by more than one order of magnitude for interchromophore distances smaller than 10 Å. Examination of the PDA between nanorods revealed an interesting dependence of the error on the intermolecular orientation: whereas for nanorods oriented on one line, the PDA underestimates the coupling by as much as a factor of 2, it overestimates the coupling between parallel oriented nanorods by as much as a factor of 3.²⁵ A similar effect was reported for the excitonic coupling between conjugated polymers.^{21,23} The enhancement/decrease of excitonic coupling by the PDA for different orientations can lead to a fortuitous error compensation in the orientational average, if both chromophores are allowed to rotate freely, as demonstrated in another computational study.²⁶ In this study, it was found that the error of the PDA dramatically increases if one of the two chromophores is kept fixed, and the other is free to rotate, as compared to the case where both are allowed to orient randomly.

Another important aspect in the calculation of the interchromophore coupling is how to take into account the polarizability of the environment, leading to local field and screening effects.^{27,28} As shown by using density functional response theory²⁹ or quantum mechanical perturbation theory,³⁰ the excitonic coupling between chromophores in a dielectric medium can be related to the classical Coulomb coupling between transition densities in a homogeneous environment with an optical dielectric constant n^2 . If two chromophores are so close that their transition densities are located in the same cavity, approximated either as an ideal sphere²⁹ or as molecule-shaped,³⁰ it was demonstrated that depending on the mutual geometry of the transition dipole moments, the Coulomb coupling might be enhanced ("in-line" geometry) or decreased (screened, "sandwich" geometry) as compared to the case without including the dielectric environment. As also discussed by Scholes et al.,³¹ this effect may depend on distance, because with increasing distance, the molecular cavities become less connected. For larger distances between chromophores, where the transition densities reside in different cavities, the presence of the second cavity can approximately be ignored when solving the Poisson equation for the electrostatic potential of the transition density in the first cavity. If, in addition, the molecular cavities are approximated by spheres and the transition densities by point dipoles located in the centers of these spheres, an analytical estimate of the screening/local field correction factor f , defined as the ratio $J(\epsilon = n^2)/J(\epsilon = 1)$ between the excitonic coupling in the medium with optical dielectric constant $\epsilon = n^2$ and in vacuum, can be obtained. In this case, f is obtained as $f = 9n^2/(2n^2 + 1)$,^{28,32} which, for the common value of $n^2 = 2$, gives a correction factor $f = 0.72$ as compared to $f = 1/n^2 = 0.5$ used in Förster theory. Because the Förster rate constant depends in second-order on the excitonic coupling, the above difference results already in a difference of a factor of 2 in the rate constant. Using molecule-shaped cavities and atomic transition charges, as in the Poisson-TrEsp method, f was found to vary between 0.5 and 0.8 for most of the couplings between chlorophyll *a* pigments in photosystem I trimers, depending on the mutual orientations of the pigments, rather than on distance.³⁰

The latter findings at first glance seem to be at odds with an earlier study, where quantum chemical calculations within the polarizable continuum model reported an exponential distance dependence of the screening factor for selected chlorophyll dimers.³¹ However, the screening constant was defined as the ratio between the coupling obtained in the medium and the coupling obtained by leaving out the direct influence of the medium on the coupling but including its effect on the oscillator strength of the pigment transitions. As demonstrated in a subsequent work by the same group,³³ the implicit effect of the medium on the oscillator strength of the pigments counterbalances its explicit effect on the coupling. Because of this effect, the screening constant defined in the usual way as the ratio between the coupling in the medium and in vacuum was found to become distance independent.³³

Probably the most critical approximation in the interpretation of FRET experiments on fluorescent labeled biomolecules with Förster theory is the assumption of the random mutual orientations of the chromophores.^{34,35} Using a PDA in the orientational averaged Förster rate constant, a $\langle \kappa^2 \rangle_{\text{orient}}$ factor appears, resulting from the orientational average over the

square of the excitonic coupling. For randomly oriented chromophores, it holds that

$$\langle \kappa^2 \rangle_{\text{orient}} = \frac{2}{3} \quad (5)$$

which is contained in the Förster radius R_0 in eq 3, whereas the κ^2 values of individual chromophore geometries vary between 0 and 4. Hence, it is clear that any restriction in the conformational flexibility of the chromophore, e.g., in its binding pocket in the protein, will lead to a nonuniform distribution of mutual orientations of chromophores and thereby to a deviation of $\langle \kappa^2 \rangle_{\text{orient}}$ from the isotropic value 2/3. This important aspect has been investigated by molecular dynamics (MD) simulations on fluorescent labeled hen egg-white lysozyme³⁶ and polyproline.^{10,37} In the case of the lysozyme study, where the orientation of one chromophore was practically fixed by its binding pocket, the $\langle \kappa^2 \rangle_{\text{orient}}$ value obtained from the MD simulations was about 30% smaller than the theoretical value obtained by taking into account one fixed dipole and one freely rotating one. In the case of polyproline, where both chromophores were flexible, the deviations between the two values was found to be about 14%. In both studies, a correlation was found between the actual distance between chromophores and the corresponding (instantaneous) κ^2 values. Taking into account this correlation, which is usually neglected, led to another 5% change in the average rate constant.³⁶

Although the effect of any one of the approximations described above has been studied in the past, how their interplay affects the interpretation of FRET experiments on fluorescent labeled proteins is less understood. The success of the standard Förster theory seems to suggest that there can be substantial error compensation between the different approximations. The present study was designed to answer this question and to provide new tools that allow experimental situations, where the standard theory is invalid, to be described, in particular, for short intermolecular distances. In our calculation scheme, the conformational flexibility of the chromophores will be described by MD simulations and the excitonic coupling for the different conformations is obtained with the Poisson-TrEsp method^{30,38} that goes beyond the PDA and includes screening and local field effects caused by the electronic polarization of the environment.

A suitable model system for this type of study is polyproline, which was used 50 years ago by Stryer and Haugland² to introduce FRET as a spectroscopic ruler. Polyproline forms a trans-helix in trifluoroethanol (TFE)^{2,37} and in water,³⁷ where in the latter case, in a fraction of complexes, a single internal proline in cis conformation occurs, as detected by nuclear magnetic resonance spectroscopy³⁷ and inferred also from fluorescence quenching by photo-induced electron transfer measured between a chromophore and a tryptophan residue attached to the termini of the polyproline helix.³⁹ Because of the internal cis conformation of a proline, the chromophores attached in FRET experiments to the ends of the polyproline helix come closer than that for all-trans polyproline. Therefore, the mean transfer efficiency measured in water is somewhat higher than that in TFE.³⁷ All-trans polyproline is relatively stiff, as predicted by early molecular mechanics calculations of conformational energies⁴⁰ and MD simulations.³⁷ Using long flexible linkers for the chromophores on one hand has the advantage of getting close to the isotropic limit for $\langle \kappa^2 \rangle_{\text{orient}}$, but on the other hand, this can lead to static disorder in

interchromophore distances that needs to be taken into account in the interpretation of the FRET experiments. The term “static” refers to all conformational transitions that are slow compared to the fluorescence lifetime of the dyes. In this way, Best et al.³⁷ finally explained a deviation between the two R_0 values that Stryer and Haugland² obtained for the polyproline system labeled with naphthyl donor and dansyl acceptor from the measured distance dependence of the energy transfer efficiency (eqs 1 and 2) and from spectroscopic data on the isolated chromophores (eq 3). A systematic investigation of the distance dependence of the FRET efficiency in polyproline labeled with Alexa dye molecules was performed by Schuler et al.¹⁴ using single-molecule experiments and ensemble time-correlated single photon measurements. Treating polyproline as a rigid rod and using Förster theory resulted in predicted FRET efficiencies that are smaller than the measured ones for long interchromophore distances (polyproline helices), whereas those predicted for small distances are larger than the experimental values. The deviations at large distances were explained by the larger flexibility of longer helices¹⁴ and by a subfraction of polyproline with internal cis residues.³⁷ For short distances, it was speculated¹⁴ that the deviations between Förster theory and experiment could be due to the breakdown of the PDA. The method introduced in the present work will allow us to analyze these deviations quantitatively.

The rest of this article is organized in the following way. First, we introduce our method combining quantum chemical, electrostatic, and MD calculations. Next, we apply this method to describe FRET experiments on polyproline helices of different lengths, containing 6, 11, 14, and 20 proline residues labeled with Alexa Fluor 488 and Alexa Fluor 594 chromophores, termed in the following as P6, P11, P14, and P20, respectively, and we compare the results with experimental data.¹⁴ Finally the results are discussed, including a detailed analysis of the different approximations that are necessary to arrive at Förster theory, and conclusions are presented.

THEORETICAL METHODS

Calculation of Excitonic Coupling. In Förster theory, a PDA is used for the excitonic coupling reading

$$J_{\text{PDA}} = \frac{\kappa \mu_{\text{D}} \mu_{\text{A}}}{n^2 R^3} \quad (6)$$

with the center-to-center distance between the chromophores R , the optical transition dipole moments of the donor and the acceptor $\boldsymbol{\mu}_{\text{D}} = \mu_{\text{D}} \mathbf{e}_{\text{D}}$ and $\boldsymbol{\mu}_{\text{A}} = \mu_{\text{A}} \mathbf{e}_{\text{A}}$, respectively, and the orientational factor

$$\kappa = \mathbf{e}_{\text{D}} \cdot \mathbf{e}_{\text{A}} - 3(\mathbf{e}_{\text{D}} \cdot \mathbf{e}_{\text{R}})(\mathbf{e}_{\text{A}} \cdot \mathbf{e}_{\text{R}}) \quad (7)$$

where \mathbf{e}_{R} is a unit vector along the connection between the centers of the two chromophores, and \mathbf{e}_{D} and \mathbf{e}_{A} are unit vectors oriented along the transition dipole moments of the donor and the acceptor, respectively. The factor $1/n^2$ in eq 6 takes into account screening of the Coulomb coupling by the optical polarizability of the environment.

In the transition charge from the electrostatic potential (TrEsp) method,²⁴ the electrostatic potentials of the ab initio transition densities of the chromophores are fitted by atomic partial charges, and the coupling is obtained from these charges as

$$J_{\text{TrEsp}} = f \sum_{I,J} \frac{q_I^{(D)} q_J^{(A)}}{|\mathbf{R}_I^{(D)} - \mathbf{R}_J^{(A)}|} \quad (8)$$

where the transition charges $q_I^{(D)}$ of the donor and $q_J^{(A)}$ of the acceptor are placed at the respective atoms I and J . The factor f describes screening and local field corrections in an implicit way.

An explicit description of these effects is obtained with the Poisson-TrEsp method.^{30,38} Here, the transition charges of the chromophores are placed in molecule-shaped cavities that are surrounded by a homogeneous dielectric with optical dielectric constant $\epsilon = n^2$, which equals the square of the refractive index and represents the electronic polarizability of the solvent. A Poisson equation is solved for the potential φ_A of the transition charges of the acceptor

$$\nabla \cdot (\epsilon(\mathbf{r}) \nabla \varphi_A(\mathbf{r})) = -4\pi \sum_J q_J^{(A)} \delta(\mathbf{r} - \mathbf{R}_J^{(A)}) \quad (9)$$

with $\epsilon(\mathbf{r}) = 1$, if \mathbf{r} points inside a chromophore cavity, and $\epsilon(\mathbf{r}) = n^2$ otherwise. The excitonic coupling between chromophores is then obtained as

$$J_{\text{P-TrEsp}} = \sum_I q_I^{(D)} \varphi_A(\mathbf{R}_I^{(D)}) \quad (10)$$

where $\varphi_A(\mathbf{R}_I^{(D)})$ is the electrostatic potential of the transition charges of the acceptor at the position of the I th transition charge $q_I^{(D)}$ of the donor.

Calculation of Rate Constant. The rate constant k of excitation energy transfer for weak excitonic coupling J between donor and acceptor reads, using Fermi's Golden Rule, $k = \frac{2\pi}{\hbar} |J|^2 D_{al}$,⁴¹ with the overlap integral D_{al} between the normalized lineshape functions of donor emission and acceptor absorption. In our calculations, we describe the rate constant as

$$k = |J|^2 C \quad (11)$$

where the excitonic coupling J is obtained from the ab initio transition density in different approximations (PDA, TrEsp, P-TrEsp) and the calibration constant C takes into account the overlap integral of the lineshape functions and, in the case of TrEsp and Poisson-TrEsp, also uncertainties in the absolute magnitude of the quantum chemical transition density, as will be described in detail below. For large intermolecular distances and isotropic orientations, the orientationally averaged rate constant is given by the Förster expression^{1,34}

$$k_F = \frac{1}{\tau_D} \left(\frac{R_0}{R} \right)^6 \quad (12)$$

with the Förster radius R_0 in eq 3, the lifetime τ_D of the excited state of the isolated donor, and the interchromophore distance R . Using eqs 5–7 and 11, we obtain

$$\frac{2}{3} \frac{(\mu_D)^2 (\mu_A)^2}{n^4 R^6} C = \frac{1}{\tau_D} \left(\frac{R_0}{R} \right)^6 \quad (13)$$

where μ_M is the magnitude of the transition dipole moment of the donor ($M = D$) or acceptor chromophore ($M = A$). Please note that we have assumed that only κ depends on the mutual orientation of the chromophores. Hence, the calibration constant follows as

$$C = \frac{3 R_0^6}{2 \tau_D} \frac{n^4}{(\mu_D)^2 (\mu_A)^2} \quad (14)$$

From the above equation, in the PDA (eq 6), the rate constant in eq 11 becomes

$$k_{\text{PDA}} = \frac{3 R_0^6}{2 \tau_d} \frac{\kappa^2(t)}{R^6(t)} \quad (15)$$

where $\kappa^2(t)$ is the square of the orientational factor κ (eq 7). Please note that the information about the magnitude of the transition dipole moment of the donor is contained in its radiative lifetime τ_D/ϕ_D and that of the acceptor in the absorption spectrum, both entering the prefactor R_0^6/τ_D in the Förster rate constant (eqs 3 and 12), which is obtained from the experimental spectroscopic properties of the isolated chromophores.

In the case of TrEsp and Poisson-TrEsp, the factor C in eq 14 also corrects for uncertainties in the absolute magnitude of the transition density. The quantum chemical transition densities are effectively rescaled such that their first moment, that is, the transition dipole moments, resemble the experimental values. The transition dipole moment of chromophore M is given as

$$\mu_M = e \sum_I \mathbf{R}_{I,0}^{(M)} q_I^{(M)} \quad (16)$$

where $q_I^{(M)}$ are the atomic transition charges obtained from a fit of the electrostatic potential of the ab initio transition density of the isolated chromophore M , and $\mathbf{R}_{I,0}^{(M)}$ is the equilibrium position of the I th nucleus of this chromophore, obtained from a geometry optimization of the whole polyproline–chromophore system, with the molecular mechanics force field used in the MD simulations. Because of slight changes of the equilibrium structure with respect to that obtained for the isolated chromophore in a quantum chemical geometry optimization, the magnitude of the transition dipoles is slightly changed for the molecular mechanics geometries. For the donor chromophore Alexa 488, the transition dipole increases from 8.2 D in the quantum chemical calculations to 8.4 D in the molecular mechanics geometry of the whole system. A similar increase, from 4.6 to 4.9 D, is obtained for the acceptor chromophore Alexa 594. For the present Alexa chromophore pair, a Förster radius $R_0 = 5.4$ nm in water ($n = 1.33$) and an excited state lifetime of the isolated donor of $\tau_D = 4$ ns were determined.¹⁴ With the transition dipole moments $\mu_D = 8.4$ D and $\mu_A = 4.9$ D, discussed above, from eq 14, a calibration constant

$$C = 0.676 \text{ cm}^{-2} \text{ ns}^{-1} \quad (17)$$

results for the present system. This calibration constant will be applied in eq 11 to calculate instantaneous rate constants k along the MD trajectories, using the TrEsp (eq 8) and the Poisson-TrEsp (eq 10) methods for the excitonic couplings.

FRET Efficiencies from Rate Constant Averages. Under stationary conditions, the populations of excited states of the donor and the acceptor n_D and n_A , respectively, are constant in time and are related by $dn_A/dt = 0 = kn_D - n_A/\tau_A$, with the excitation energy transfer rate constant k and where $\tau_A^{-1} = (\tau_A^{\text{rad}})^{-1} + (\tau_A^{\text{nr}})^{-1}$ comprises radiative and nonradiative decay processes between the excited and the ground state of the acceptor. Hence, the relative population of excited states of the donor and the acceptor under stationary conditions is

$$\frac{n_D}{n_A} = \frac{1}{k\tau_A} \quad (18)$$

The field intensities of the donor and acceptor fluorescence follow as $I_{D/A}^{(F)} \propto n_{D/A}/\tau_{D/A}^{\text{rad}}$, and the detectors measure the intensities $I_{D/A} \propto \sigma_{D/A} I_{D/A}^{(F)}$, where σ_D and σ_A are the sensitivities of the detectors for the donor and acceptor photons, respectively. Hence, the relative intensities are given as

$$\frac{I_D}{I_A} = \frac{n_D}{n_A} \frac{\tau_A^{\text{rad}}}{\tau_D^{\text{rad}}} \frac{\sigma_D}{\sigma_A} \quad (19)$$

which, using eq 18, becomes

$$\frac{I_D}{I_A} = \frac{1}{\tau_A k} \frac{\tau_A^{\text{rad}}}{\tau_D^{\text{rad}}} \frac{\sigma_D}{\sigma_A} = \frac{\phi_D}{\phi_A} \frac{\sigma_D}{\tau_D k} = \frac{1}{\gamma \tau_D k} \quad (20)$$

with $\gamma = \phi_A \sigma_A / (\phi_D \sigma_D)$ introduced in eq 1, where the fluorescence quantum efficiencies $\phi_{D/A}$ are defined as $\phi_{D/A} = \tau_{D/A} / \tau_{D/A}^{\text{rad}}$. τ_D in eq 20 is the excited state lifetime of the donor in the absence of the acceptor and comprises radiative and nonradiative processes. With eq 20, the energy transfer efficiency in eq 1 is obtained as

$$E = \frac{1}{1 + \frac{1}{\tau_D k}} \quad (21)$$

Depending on the relative timescale of energy transfer/fluorescence decay and conformational dynamics, two limiting scenarios can be distinguished. If the conformational dynamics of the chromophores is fast compared to their fluorescence lifetime, the emitted photons have averaged over the different mutual orientations and an average rate constant $\langle k \rangle$ appears in the measured efficiency $E_f = \left(1 + \frac{1}{\tau_D \langle k \rangle}\right)^{-1}$. In the limit where the conformational transitions are slow, the emitted photons measure the efficiencies of the different (static) conformations and the overall efficiency is given as $E_s = \left\langle \left(1 + \frac{1}{\tau_D k}\right)^{-1} \right\rangle$. In the analysis of our MD trajectories, we take into account the fluctuations that are fast compared to the excited state lifetime of the chromophores by an average of the rate constant and those which are slow by an average of the efficiency. The overall efficiency is then obtained as

$$E = \left\langle \left(1 + \frac{1}{\tau_D \langle k \rangle_f}\right)^{-1} \right\rangle_s \quad (22)$$

where $\langle \dots \rangle_f$ denotes an average of the instantaneous rate constant $k(t)$ over the fast fluctuations

$$\langle k(t) \rangle_f = \frac{1}{\tau_D} \int_{t-\tau_D/2}^{t+\tau_D/2} dt' k(t') \quad (23)$$

and $\langle \dots \rangle_s$ describes an average of the efficiencies with respect to static disorder, that is, conformational substates, with lifetimes that are longer than the excited state lifetime of the chromophores. In our simulations, we run several MD trajectories for randomly chosen initial conditions, perform the average in eq 23 for every trajectory separately, and afterwards, combine all trajectories and perform the average over static disorder of the whole ensemble. The above distinction between fast and slow fluctuations will be checked

by performing Monte Carlo (MC) simulations of FRET efficiencies, described further below.

With the PDA rate constant k_{PDA} in eq 15, the FRET efficiency in eq 22 becomes

$$E_{\text{PDA}} = \left\langle \left(1 + \frac{2}{3R_0^6} \left\langle \frac{R^6}{\kappa^2} \right\rangle_f \right)^{-1} \right\rangle_s \quad (24)$$

where the interchromophore distance $R(t)$ and orientational factor $\kappa(t)$ are obtained from the MD simulations. In the case of the Poisson-TrEsp couplings (eq 10) and the TrEsp couplings (eq 8), the rate constant $k(t)$ entering the FRET efficiency in eq 22 is obtained from eqs 11 and 17.

The FRET efficiencies, calculated as described above, will be compared with experimental results from single-molecule spectroscopy.¹⁴ In the latter case, distribution functions are obtained with a width that is largely determined by the shot noise resulting from the finite number of photons collected, and to a minor extent, by the mixture of all-trans polyproline with polyproline containing a cis conformation. For polyproline 20, it has been estimated that in 30% of the peptides, a single internal cis residue is present somewhere along the helix.³⁷ In the present work, for simplicity, we investigate only all-trans polyproline, but provide an estimate of the influence of the missing contribution to the efficiency resulting from internal cis conformations. Because the photons are collected with ms time-resolution,^{14,37} except for the cis–trans conformational change occurring on a longer timescale,³⁹ there is complete conformational averaging over the mutual geometries of the two chromophores during the observation time of a single molecule. Furthermore, we do not include the shot noise because it does not critically affect the average efficiencies, which were found to agree with efficiencies obtained from the time-correlated ensemble experiments.¹⁴ A detailed investigation of the distribution functions measured in single-molecule FRET experiments is a highly non-trivial task^{4,10,37} and is beyond the scope of the present work.

FRET Efficiencies from Monte Carlo Simulations. To check the validity of eq 22 for the efficiency derived above, where we have separated the slow from the fast fluctuations in the respective averages, direct Monte Carlo (MC) simulations¹⁰ of the efficiencies along the MD trajectories, from which the instantaneous rate constants $k(t)$ are obtained, are performed. These MC calculations consist of an outer and an inner run. In the outer run on a given MD trajectory, an initial starting time t is chosen randomly, from where the inner MC run is started. The latter is performed along the MD trajectory providing the time-dependent rate constant $k(t)$ in time steps of Δt . We assume that a photon was absorbed by the donor at this initial time t . We now distinguish between the probability $p_D = \Delta t / \tau_D$ that the donor gets de-excited by photon emission, the time-dependent probability $p_A(t) = k(t) \Delta t$ that the excitation energy of the donor is transferred to the acceptor, and the probability $1 - p_D - p_A(t)$ that the donor stays excited within the next time step Δt , as illustrated in Figure 1. In the inner MC run, a particular realization of events is obtained by picking a random number X that is uniformly distributed in the interval between 0 and 1. This interval is divided according to the three probabilities discussed above. If X is smaller than p_D , the donor emits a photon and a new outer MC run is started. If X is larger than p_D and smaller than $p_D + p_A(t)$, there is excitation energy transfer to the acceptor and the acceptor emits a photon. Again,

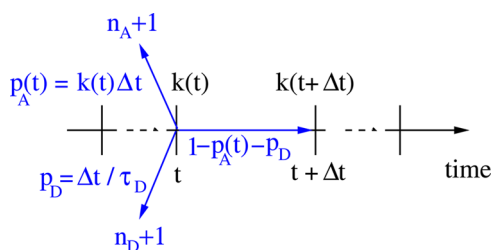


Figure 1. Illustration of Monte Carlo procedure described in the text.

the outer MC run is restarted by choosing a new initial time t . If X is larger than $p_D + p_A(t)$, the donor stays excited and the system moves to the next point $t + \Delta t$ in time, that is, the instantaneous rate constant $k(t)$ used in the previous step is replaced by $k(t + \Delta t)$, and a new random number X is taken and the next event determined, accordingly. This procedure is continued until either a donor or an acceptor photon is emitted. Afterwards, a new outer MC run is started. The FRET efficiency then follows from the total numbers n_D and n_A of donor and acceptor photons, respectively, as

$$E = \frac{n_A}{n_A + \gamma n_D} \quad (25)$$

where the factor γ takes into account the different fluorescence quantum yields of the donor and the acceptor and the different sensitivities of the detectors of the donor and acceptor photons, as before. The outer MC run is repeated until the efficiency E is converged.

Finally, we note that the MC procedure described above includes the limiting cases of dynamic and static disorder, where the fluctuations of the rate constant are fast and slow, respectively, compared to the excited state lifetime of the donor, as well as all intermediate regimes. In the case of fast fluctuations, the inner MC run on average will sample many different rate constants before a photon is emitted; whereas for slow fluctuations, every excited donor state has just seen one FRET rate constant and the outer MC run alone determines the disorder.

Estimation of Contribution from Internal Cis Residues to the Efficiency. NMR experiments³⁷ have shown that there is a small percentage of polyproline helices containing cis prolines, where the probability p_c of such a cis conformation was found to be 10% for the C-terminal proline and $p_c = 2\%$ for the remaining prolines, termed internal in the following. Hence, the probability of finding a polyproline helix with k internal residue in cis conformation is given as¹⁰

$$p_{k\text{-cis}}^{(N)} = \binom{N-1}{k} p_c^k (1-p_c)^{(N-1-k)} \quad (26)$$

The probabilities resulting for one and two cis conformations are listed in Table 1 for the polyprolines investigated here ($N = 6, 11, 14, 20$). The probabilities for more than two cis residues is negligible ($<1\%$). The single-molecule experiments for $N = 20$ in water and in TFE solvent, where no internal cis residues in polyproline are formed, have revealed that there is an efficiency increase by 0.1 due to the internal cis residues from $E_t^{(20)} = 0.51$ in TFE³⁷ to $E_c^{(20)} = 0.61$ in water.^{14,37} We have used the efficiencies extracted for $\gamma = 1$ (eq 1) in ref 37 from experimental data on P20 to be consistent with the efficiencies extracted in ref¹⁴ for the different helices considered in this work.

Table 1. Probabilities $p_{k\text{-cis}}^{(N)}$ (Equation 26) To Find $k = 1$ and 2 Internal Cis Conformations in a Polyproline Helix of Length N and Resulting Increase in FRET Efficiency ΔE_N ^a

N	$p_{1\text{-cis}}^{(N)}$ (%)	$p_{2\text{-cis}}^{(N)}$ (%)	ΔE_N
6	13.9	1.0	0.002
11	16.7	1.6	0.014
14	20.4	2.5	0.039
20	26.4	4.9	0.1

^aEstimated as described in the text (eq 29).

The increase in efficiency in the presence of cis residues is due to the smaller interchromophore distance. Using the Förster expression for $R(E)$ in eq 4, the decrease in average distance for this system can be estimated as

$$\Delta R_{20} = R(E_t^{(20)}) - R(E_c^{(20)}) \quad (27)$$

which results in $\Delta R_{20} = 3.5 \text{ \AA}$ for the present system.

For geometrical reasons, we estimate the average distance decrease of the other ($N = 9, 11, 14$) polyprolines as

$$\Delta R_N = \Delta R_{20} \frac{R_t^{(N)} P_{\text{cis}}^{(N)}}{R_t^{(20)} P_{\text{cis}}^{(20)}} \quad (28)$$

where $R_t^{(N)}$ is the average interchromophore distance obtained for the N -proline all-trans helix in our MD simulations (2nd column of Table 2) and $P_{\text{cis}}^{(N)} = \sum_k p_{k\text{-cis}}^{(N)}$ is the probability to find at least one internal cis residue in the helix. From this decrease in average distance, using $E(R)$ in eq 2, an increase of the efficiency

$$\Delta E_N = E_c^{(N)} - E_t^{(N)} = E(R_t^{(N)} - \Delta R_N) - E(R_t^{(N)}) \quad (29)$$

results, which is used to obtain an estimate for the efficiency of those polyproline helices with all internal trans conformations, for which no direct experimental data are available. The numerical values for ΔE_N are given in Table 1 (last column). Whereas there is a significant increase of the experimental efficiency for the longest helix P20 due to the internal cis residues, the influence of the latter is practically zero for the shortest helix P6. Finally, we note that there are no experiments on polyproline without the small fraction of C-terminal cis conformations. Modeling studies³⁹ show that a cis conformation at the end of a helix has a much weaker influence on the interchromophore distance than one in the center, as expected. Indeed, MD simulations with and without C-terminal cis residues obtained a very similar decay of the donor fluorescence by FRET.³⁷ In the present analysis, therefore, we neglect the influence of these C-terminal cis conformations.

COMPUTATIONAL DETAILS

Molecular Dynamics Simulations. The conformational dynamics of all-trans polyproline helices of 6, 11, 14, and 20 proline residues labeled with Alexa 594 and Alexa 488 dyes in aqueous solution was studied with all-atom MD simulations.¹⁰ The system was dissolved in a water box filled with 300 mM NaCl, which equals the ionic strength of 50 mM sodium phosphate buffer used in the experiment.¹⁴ For polyproline, we used the standard molecular mechanics CHARMM force field (version v35b3).^{42,43} The parameters of the force fields of the Alexa chromophores were created by an analogy approach from that of similar chemical groups in the CHARMM force field^{42,43} (respective parameter files can be downloaded from the

Table 2. FRET Efficiencies E Obtained in Different Approximations as a Function of the Average Interchromophore Distance $\langle R \rangle$ for Helices with Different Number N of Polyprolines in Comparison to Experimental Values E_{exp}^{14} and $E_{\text{exp}}^{(\text{corr})\alpha}$

N	$\langle R \rangle$ (Å)	E_{exp}	$E_{\text{exp}}^{(\text{corr})}$	$E_{\text{P-TrEsp}}$	E_{TrEsp}	E_{PDA}	$E_{\text{PDA}}^{(R^*)}$	$E_{\text{PDA}}^{(R^{\text{iso}})}$	$E_{\text{PDA}}^{(F)}$
6	25.3	0.93	0.93	0.93	0.93	0.92	0.91	0.94	0.99
11	34.7	0.86	0.85	0.84	0.84	0.81	0.78	0.87	0.93
14	42.5	0.81	0.77	0.77	0.77	0.73	0.70	0.76	0.81
20	56.8	0.61	0.51	0.46	0.46	0.46	0.41	0.43	0.42

$E_{\text{exp}}^{(\text{corr})}$ was corrected for the presence of internal cis residues, as described in the text (eq 29, Table 1). $E_{\text{P-TrEsp}}$ and E_{TrEsp} were obtained from eqs 22 and 11 using either eq 10 or 8, respectively, for the couplings. The expressions for the PDA efficiencies E_{PDA} , $E_{\text{PDA}}^{(R^*)}$, $E_{\text{PDA}}^{(R^{\text{iso}})}$ and $E_{\text{PDA}}^{(F)}$ are given in eqs 24 and 31–33, respectively.

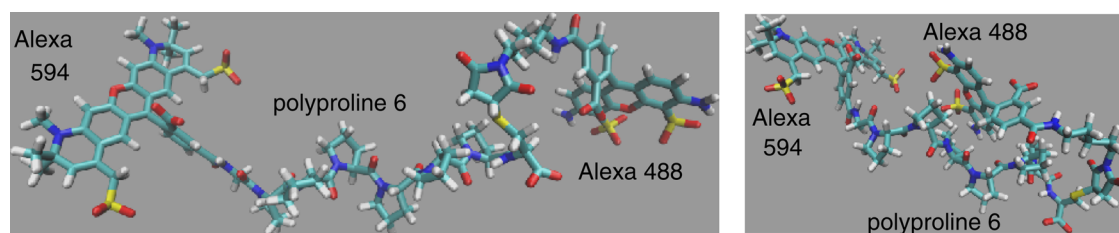


Figure 2. Structure of polyproline 6 labeled with Alexa 488 and Alexa 594 chromophores in open (left part) and closed (right part) conformations, obtained from two snapshots of a MD simulation with explicit waters (not shown).

Supporting Information (SI)). The water molecules of the aqueous environment were explicitly included using a TIP3P parameterization.⁴⁴ The MD simulations were performed with the NAMD software package.⁴⁵ First, polyproline, labeled with Alexa dyes, was geometry optimized, using as a starting structure an all-trans polyproline helix with backbone dihedral angles $\phi = -75^\circ$ and $\Psi = 150^\circ$. Periodic boundary conditions were applied in all dimensions. The initial conformations for the trajectories were obtained after a 5 ns equilibration run. The trajectories were propagated with a 2 fs time step, at a constant temperature 300 K and NPT conditions. The constant pressure control was enabled by a Langevin piston with period 100 fs and decay time constant 50 fs. The cut-off distance for electrostatic and van der Waals interactions was set to 12 Å. For the calculation of long-range electrostatic interactions, the particle-mesh-Ewald method was employed. For each polyproline length, we generated 10 trajectories, each with a time window of 200 ns. Two snapshots of the MD simulation on P6 are shown in Figure 2. In the structure shown in the left part, the distance between chromophores is large, and in that in the right part, it is small, representing an “open” and a “closed” conformation. In the latter, the long flexible linker of the donor chromophore Alexa 488 is directed back onto the polyproline helix and the chromophore comes in contact with the helix, as noted also in earlier modeling studies.^{10,12}

Quantum Chemical/Electrostatic Calculations. The geometry of the isolated chromophores was optimized by density functional theory (DFT) calculations using the B3LYP exchange-correlation (XC) functional and a 6-31G* basis set with the program Jaguar.⁴⁶ On the basis of this geometry, the transition density between the ground state and the first excited state of the chromophores and the corresponding electrostatic potentials were calculated using the Hartree–Fock/configuration interaction with single excitations method and a 6-31G* basis set, with the program Q-CHEM.⁴⁷ Atomic transition charges were obtained by fitting the ab initio electrostatic potential of the transition density on a 3D grid around the chromophores using the program CHELP-BOW.⁴⁸ Numerical values of the transition charges of the chromophores are given in the SI. These charges were placed at the respective

atom positions obtained from the MD simulations. In the Poisson-TrEsp method, the Poisson equation (eq 9) for the electrostatic potential of the transition charges in molecule-shaped cavities embedded in a homogeneous dielectric was solved numerically every 10 ps along the MD trajectories using the program MEAD.⁴⁹ In the TrEsp method, the excitonic couplings were obtained directly from the Coulomb coupling (eq 8) between transition charges of the two chromophores, first in vacuum ($f = 1$) and later in the medium by introducing an effective dielectric constant ($f = 1/\epsilon_{\text{eff}}$) based on the comparison with the Poisson-TrEsp couplings. In the PDA, first, the magnitude and direction of the transition dipoles of the chromophores in the molecular frames were obtained by placing the quantum chemical transition charges onto the equilibrium structure resulting from the molecular mechanics force field, as described above (eq 16). The transition dipole of Alexa 488 was found to be oriented parallel to the line connecting atoms C24 and C28, and that of Alex 594 is oriented parallel to the connection between atoms C24B and C28B (the position of these atoms is defined in the SI). During the MD simulations, the direction of the transition dipoles was obtained from the positions of those four atoms and the resulting point dipoles were placed at the centers of the central rings of the conjugated π -systems of the chromophores (see SI). Finally, the Coulomb coupling between point dipoles was calculated using eqs 6 and 7. The TrEsp and PDA couplings were evaluated every 500 fs along the MD trajectories.

RESULTS

In Figure 3, correlation plots are presented of excitonic couplings obtained along the 2 μs MD trajectories for the four polyproline helices (P6, P11, P14, and P20) investigated in this work. To investigate the validity of the PDA, we have correlated the PDA couplings with the TrEsp couplings (in vacuum) in the right half of Figure 3. For the shortest helix P6, there is significantly less correlation than for the longer helices P11–P20, illustrating the shortcomings of the PDA at close interchromophore distances. The correlation is largest for the longest helix (P20), as expected.

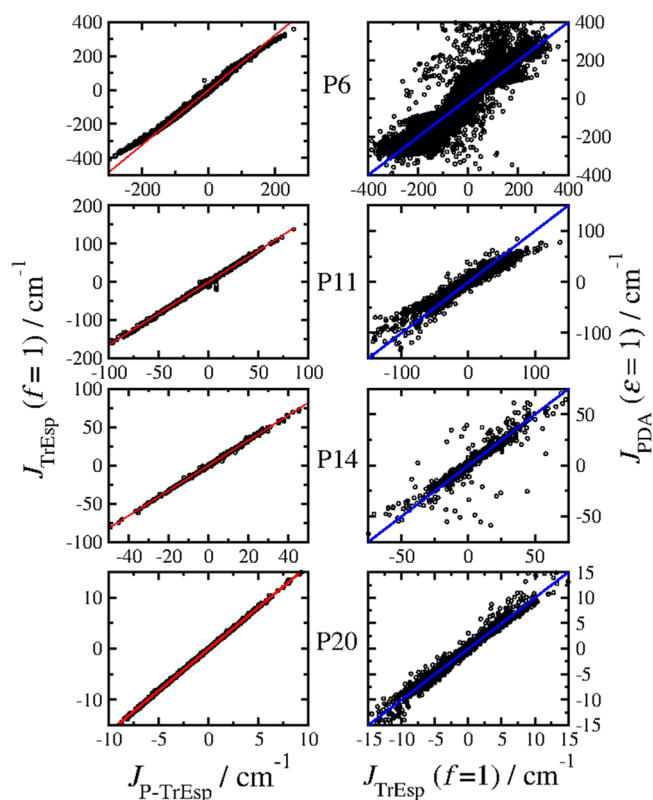


Figure 3. Correlation of excitonic couplings obtained with different methods along the MD trajectories of polyprolines 6, 11, 14, and 20 from top to bottom. The left half contains the correlation between the TrEsp couplings (eq 8 for $f = 1$) and the Poisson-TrEsp couplings (eq 10). The red solid lines are obtained from a linear regression. The right half contains the correlations between the PDA couplings (eq 6) and the TrEsp couplings (eq 8), both calculated in vacuum. The blue solid lines indicate a perfect correlation between the two types of couplings.

An excellent correlation between the TrEsp couplings in vacuum (eq 8 with $f = 1$) and the Poisson-TrEsp couplings in water (optical dielectric constant $\epsilon = n^2 = 1.77$) (eq 10) was obtained for all helix lengths, as shown in the left half of Figure 3. The correlation is slightly weaker for the shortest helix P6 at high absolute magnitudes of the couplings. From the ratio between the vacuum coupling obtained with TrEsp and the Poisson-TrEsp couplings in water, we define an effective dielectric constant as

$$\epsilon_{\text{eff}} = \frac{J_{\text{TrEsp}}(f = 1)}{J_{\text{P-TrEsp}}(\epsilon = 1.77)} \quad (30)$$

The resulting probability densities of ϵ_{eff} are shown in Figure 4. Very similar results are obtained for the different helices. From the peak position of these distribution functions, we estimate an effective dielectric constant $\epsilon_{\text{eff}} \approx 1.65$, which will be used in the calculation of FRET efficiencies with the TrEsp method below.

The FRET efficiencies obtained from eqs 11 and 22 with the Poisson-TrEsp couplings (eq 10) and TrEsp couplings (eq 8, $f = 1/\epsilon_{\text{eff}}$, $\epsilon_{\text{eff}} = 1.65$) and from eq 24 for PDA couplings are shown as a function of average interchromophore distance in Figure 5. These efficiencies are compared to the experimental values¹⁴ and the prediction of Förster theory (eq 2). The original experimental values E_{exp} are shown, as well as those that were corrected for the presence of internal cis residues $E_{\text{exp}}^{(\text{corr})} =$

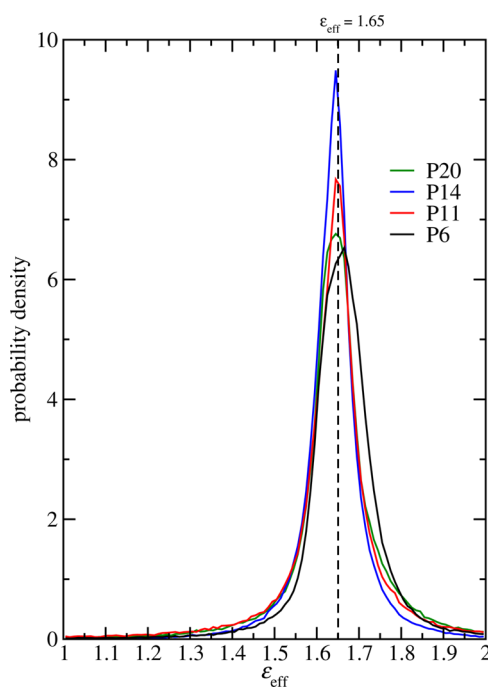


Figure 4. Probability density of an effective dielectric constant defined in the text (eq 30) for four different helices: P6 (black), P11 (red), P14 (blue), and P20 (green). The vertical dashed line in the upper part denotes the most likely value for the effective dielectric constant $\epsilon_{\text{eff}} = 1.65$, which is used in the calculation of FRET efficiencies with the TrEsp method (eq 8 with $f = 1/\epsilon_{\text{eff}}$).

$E_{\text{exp}} - \Delta E_N$ with the ΔE_N estimated as described above (eq 29, Table 1). Because our MD simulations were done only on all-trans polyproline, we will compare our results with $E_{\text{exp}}^{(\text{corr})}$ in the following and will refer to these values as experimental values.

As noted already in the experimental paper,¹⁴ the experimental efficiencies for short helices are below the predictions of Förster theory. The present Poisson-TrEsp/MD and the simpler TrEsp/MD methods provide quantitative agreement with the experimental values for short and intermediate helix lengths (P6, P11, and P14) and a somewhat too low efficiency for the longest helix (P20). Interestingly, the PDA/MD FRET efficiencies are also close to the experimental data, in particular, for the shortest helix P6, where the PDA for the individual conformations starts to become invalid, as the low correlation with the TrEsp couplings for P6 shows (right top part of Figure 3). The PDA/MD FRET efficiencies for the intermediate helix lengths (P11 and P14) are somewhat below the efficiencies obtained with Poisson-TrEsp/MD and TrEsp/MD, whereas for the shortest helix P6 and the longest helix P20, all three methods practically give the same result. Obviously, the PDA is not responsible for the overestimation of FRET efficiency obtained by Förster theory for short and intermediate interchromophore distances.

We checked our approximation to divide the ensemble average into an average of the rate constant over the fast fluctuations and an average of the efficiencies over the slow fluctuations (eq 22). For this purpose, we performed MC calculations that directly include the fast and slow fluctuations of the instantaneous rate constant, as described above. For these calculations, the TrEsp rate constants were used, which are available at a step size of $\Delta t = 500$ fs along the MD trajectories. We used this Δt for the inner run in the MC calculations. Convergence of the computed efficiencies was

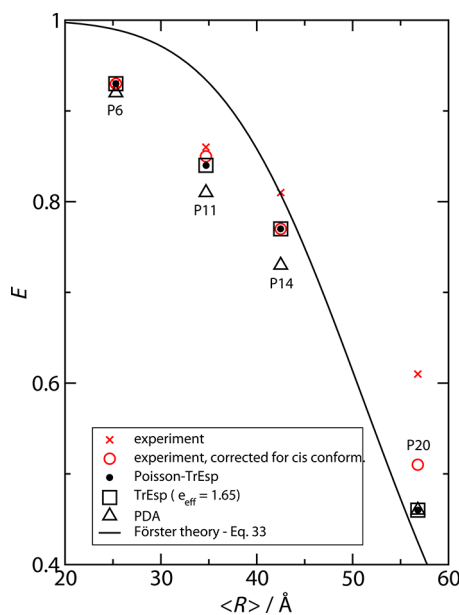


Figure 5. FRET efficiencies E as a function of mean interchromophore distance $\langle R \rangle$ (obtained from the MD simulations) calculated with different excitonic couplings (black symbols) are compared to experimental data (red symbols) and predictions from Förster theory (black line). The excitonic couplings have been calculated along the nuclear trajectories obtained with MD simulations using the Poisson-TrEsp method (filled black circles), the TrEsp method with $\epsilon_{\text{eff}} = 1.65$ (open black squares), and the PDA (open triangles). The original experimental values¹⁴ (red X) are corrected for the presence of a small amount of internal cis residues, as described in the text (eq 29, Table 1). The corrected experimental values are shown as open red circles. For P6, all symbols overlap, and for P20, all black symbols (representing the theoretical results) overlap. The numerical values of the data points in this graph are given in Table 2.

obtained after 10^6 outer MC runs. The calculated MC efficiencies are in excellent agreement with the results obtained from eq 22, as shown in Figure 6.

An advantage of the averaged rate constants is that we can systematically bridge the gap between the PDA/MD result and the predictions of Förster theory by neglecting certain

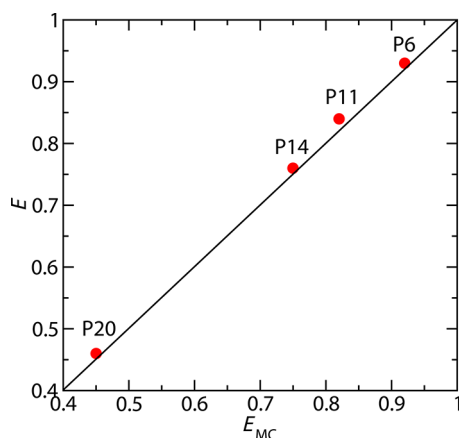


Figure 6. Correlation between the efficiency E obtained from the averaged rate constants (eq 22) and the efficiency E_{MC} obtained from MC calculations using the instantaneous rate constants. The TrEsp couplings have been used to calculate the rate constants. The solid line indicates a perfect correlation.

correlations in this average, as will be shown in the following. In the case of uncorrelated fast fluctuations of κ^2 and R^6 , the expression for the PDA/MD efficiency in eq 24 becomes

$$E_{\text{PDA}}^{(R,\kappa)} = \left\langle \left(1 + \frac{2}{3R_0^6} \frac{\langle R^6 \rangle_f}{\langle \kappa^2 \rangle_f} \right)^{-1} \right\rangle_s \quad (31)$$

By setting $\langle \kappa^2 \rangle_f = 2/3$, we assume isotropic mutual orientations of the chromophores and obtain the efficiency

$$E_{\text{PDA}}^{(R,\text{iso})} = \left\langle \left(1 + \frac{\langle R^6 \rangle_f}{R_0^6} \right)^{-1} \right\rangle_s \quad (32)$$

Finally, we arrive at the Förster expression for the efficiency by also including the slow fluctuations into the average of the interchromophore distance and by setting $\langle R^6 \rangle_{f+s} = \langle R^6 \rangle \approx \langle R \rangle^6$. The resulting efficiency reads

$$E_{\text{PDA}}^{(F)} = \frac{1}{1 + \frac{\langle R \rangle^6}{R_0^6}} \quad (33)$$

where $\langle R \rangle$ is the average interchromophore distance that has to be identified with the distance R in eq 2 of Förster theory. The efficiencies obtained on the different levels of approximation for P6, P11, and P14 are shown in Figure 7, including also the

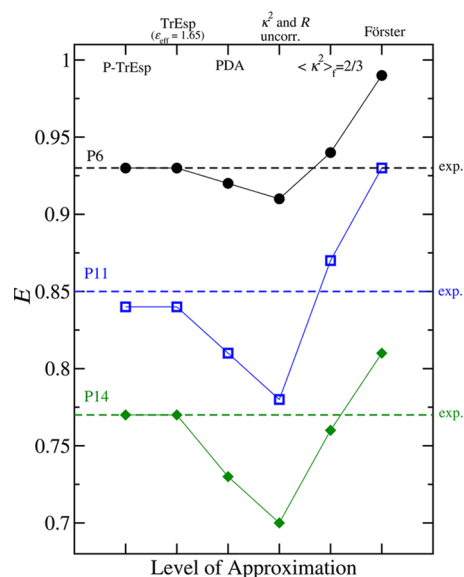


Figure 7. Comparison of FRET efficiencies for P6 (black), P11 (blue), and P14 (green) obtained in different approximations (from left to right: (i) Poisson-TrEsp (eqs 10, 11, and 22), (ii) TrEsp (eqs 8, 11, and 22, $f = 1/\epsilon_{\text{eff}} = 1/1.65$), (iii) PDA (eq 24), (iv) PDA neglecting the correlation between κ^2 and R^6 (eq 31), (v) PDA assuming isotropic mutual orientations of chromophores by setting $\langle \kappa^2 \rangle = 2/3$ (eq 32), and (vi) standard Förster theory (eq 33)). The experimental efficiencies are shown as horizontal dashed lines. The numerical values of the data points in this graph are given in Table 2.

more accurate P-TrEsp and TrEsp results as well as the experimental values. For all helices, there is a nonmonotonic dependence of the FRET efficiency on the level of approximation. Whereas the PDA and the neglect of correlations in interchromophore distances and orientations decrease the FRET efficiencies, this decrease is overcompensated

sated by the neglect of static disorder in interchromophore distances and orientations. Hence, the latter two approximations are responsible for the overestimation of the FRET efficiencies by Förster theory for the present system.

There is indeed a considerable amount of static disorder in the interchromophore distances and mutual orientations of chromophores, as demonstrated by the distribution functions of the orientational factor κ^2 and the interchromophore distance R , both averaged over the fluorescence lifetime, shown in Figure 8. For comparison, we have included the distribution

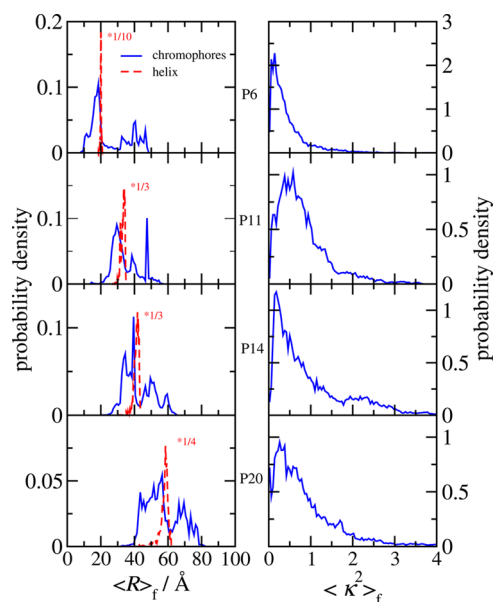


Figure 8. Probability density of interchromophore distance and helix length (blue and red curves, respectively, in left half), orientational factor $\langle \kappa^2 \rangle_f$ of PDA (right half), all averaged over the fast fluctuations (as in eq 23) for the different polyproline helices (from top to bottom): P6, P11, P14, and P20. The red curves in the left half have been scaled down as indicated by the red numbers for better comparison.

function of the helix length, which is very sharp compared to the distribution function of interchromophore distances. Whereas the polyproline helix is rather stiff, the long flexible linker of the donor chromophore Alexa 488 leads to large variations in interchromophore distances. In the case of the shortest helix P6, these variations are similar to the helix length, as illustrated also in Figure 2, where two snapshots are shown, representing the open and the closed conformation, with large and small interchromophore distances, respectively.

DISCUSSION

The aim of the FRET experiments is to extract distances from measured energy transfer efficiencies. Despite the long linker of the donor chromophore Alex 488, the average interchromophore distance and the average helix length agree quite well (first and second row in Table 3). Hence, FRET for this system represents a valid ruler for the helix length. The good quantitative agreement between the experimental energy transfer efficiencies with those calculated based on the present combination of MD simulations of the nuclear trajectories and the Poisson-TrEsp calculation of excitonic couplings provide evidence that the MD simulations create a representative ensemble of the conformational substates of the present system.

Table 3. Average Helix Length $\langle R_{\text{helix}} \rangle$ and Interchromophore Distance $\langle R \rangle$ Obtained from MD Simulations for the Different Polyproline Helices of Length N As Compared to Distances $R(E_{\text{exp}}^{\text{corr}})^a$

N	MD		Förster
	$\langle R_{\text{helix}} \rangle$	$\langle R \rangle$	$R(E_{\text{exp}}^{\text{corr}})$
6	20.0	25.3	35.1
11	34.1	34.7	40.4
14	42.2	42.5	44.2
20	59.1	56.8	53.6

^aEstimated from experimental efficiencies $E_{\text{exp}}^{\text{corr}}$ (corrected for internal cis residue, Table 2, fourth column) using Förster theory (eq 4, $R_0 = 54 \text{ \AA}$). All distances are given in units of Ångstrom.

Therefore, it is instructive to compare the interchromophore distances obtained from MD with those that follow directly from the experimental efficiencies using Förster theory. For the two longer polyproline helices, those two distances agree within a 5% error margin (second and third rows of Table 3). For the shortest helix, a 30% deviation between the average MD interchromophore distance and the distance predicted by Förster theory is obtained, and for the second shortest helix P11, the deviation is still 15%. At first glance from Figure 3 (right top part), it seems obvious that the limitation of the PDA is responsible for the large error of P6. However, a detailed analysis of the different levels of approximation connecting the MD/Poisson-TrEsp analysis with Förster theory in Figure 7 reveals that the PDA alone even leads to a slight decrease of the efficiency and, therefore, this cannot explain the overestimation of the FRET efficiency by Förster theory resulting in an overestimation of the interchromophore distance. Instead, in Förster theory, the drop in efficiency by applying a PDA and by assuming uncorrelated distance and orientation factors is overcompensated by the assumption of a single isotropic orientational factor $\langle \kappa^2 \rangle_f = 2/3$ and by the neglect of the distribution in interchromophore distances. The latter two approximations are not only invalid for P6 but also for the longer helices, as Figure 8 demonstrates. In Förster theory, the chromophores are assumed to sample their conformational space quickly compared to their fluorescent lifetime and hence the distribution functions of interchromophore distances and orientations in Figure 8 should just show a sharp single peak located at the average interchromophore distance and at $\langle \kappa^2 \rangle_f = 2/3$, respectively. In contrast, very broad distribution functions are obtained. The neglect of the finite width of these distribution functions for $\langle \kappa^2 \rangle_f$ and $\langle R \rangle_f$ is responsible for the overestimation of the energy transfer efficiency for P6, P11, and P14 by Förster theory in Figure 5. The error in inferred interchromophore distance for P6 and P11 is enlarged by the smaller slope of the Förster theory efficiency-versus-distance curve for small distances (Figure 5). For P14 and P20, the good quantitative agreement between the prediction of Förster theory and the interchromophore distances obtained from MD relies on error compensation (Figure 7) and the steep slope of the efficiency-versus-distance curve (Figure 5). The error compensation between different approximations of Förster theory is a remarkable result of the present work. For example, in the case of P11, the absolute magnitudes of the errors between different levels of approximation in Figure 7 add up to 0.21 efficiency units, whereas the actual error of Förster theory with respect to P-TrEsp/MD is just 0.07 units, due to the different signs of individual errors of the underlying

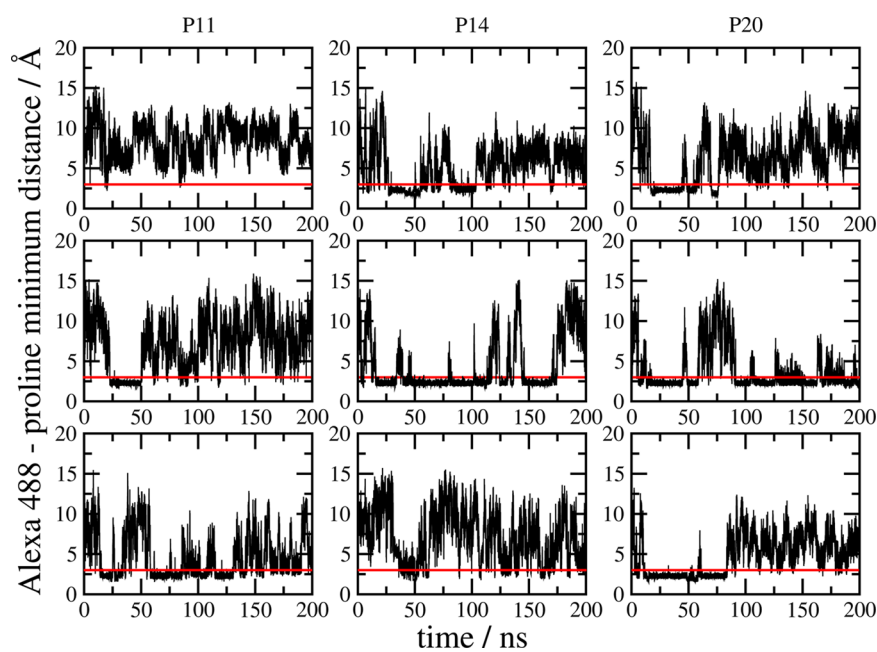


Figure 9. Closest interatomic distance between the Alexa 488 chromophore and the polyproline helix along three representative 200 ns trajectories for polyproline helices P11 (left), P14 (middle), and P20 (right). The red horizontal lines refer to a distance of 3 Å used to define the bound state of the chromophore.¹²

approximations. This deviation is only about a factor of 2 larger than the minimal experimental error (0.02 to 0.05 efficiency units) in single-molecule FRET experiments, estimated in a benchmark study recently,¹³ based on independent experiments performed in 20 different laboratories worldwide.

A critical extension of the standard theory, essential for the present analysis, was to go beyond the PDA and the simple $1/n^2$ screening model for the calculation of excitonic couplings. The Poisson-TrEsp method is ideally suited for this purpose because it is accurate, numerically efficient, and robust against distortions of molecular conformations, obtained here from classical MD simulations. Interestingly, the efficiency calculated with PDA couplings for the shortest helix P6 agrees quite well with that obtained for the Poisson-TrEsp couplings (Figure 5), despite the fact that the individual PDA couplings for P6 are not very accurate, as the correlation with the TrEsp couplings (right top part in Figure 3) demonstrates. Obviously, there is also an error compensation in the average over the different conformations leading to the FRET efficiency. A similar effect was noted already in earlier quantum chemical calculations,²⁶ as discussed in the Introduction. Interestingly, this error compensation works somewhat less well for the intermediate helix lengths P11 and P14, despite the much better correlation between the individual PDA and TrEsp couplings (right middle parts in Figure 3). For the longest helix P20, the PDA couplings of the individual conformations are accurate enough that no error compensation is needed to give quantitative agreement between the resulting efficiency and those obtained with the Poisson-TrEsp and the TrEsp methods.

The numerical bottleneck of the Poisson-TrEsp method is the solution of a Poisson equation for the electrostatic potential of transition charges of the chromophores. The excellent correlation between Poisson-TrEsp couplings and the TrEsp results (left column in Figure 3) suggests that the local field correction and screening effects can be approximated by screening the vacuum couplings by an effective dielectric constant, which for the present system amounts to $\epsilon_{\text{eff}} \approx 1.65$,

rather independent of chromophore distance and relative orientation of the chromophores (Figure 4). This aspect dramatically reduces the numerical effort because the solution of a Poisson equation can be avoided to a large extent. To determine the value ϵ_{eff} however, at least some molecular conformations need to be analyzed with Poisson-TrEsp. The analytical model approximating the molecules as spheres and the transition density by a point dipole, discussed in the Introduction, predicts an effective screening constant $\epsilon_{\text{eff}} = 1.29$, which does not explain our numerical result $\epsilon_{\text{eff}} = 1.65$ for the present system. The independence of this screening constant of interchromophore distance and orientation (Figure 3) is striking. For the shortest helix P6, in the closed conformation (right part in Figure 2), the distance between atoms in different chromophores can get as small as 3.5 Å, and hence the two molecule-shaped cavities become very close. In such situations, depending on the mutual orientation of chromophores, an enhancement or a decrease of ϵ_{eff} has been reported earlier,^{29,30} including the Poisson-TrEsp study on photosystem I.³⁰ It seems that for the present system P6, the closed conformation, for which small interchromophore distances occur, has led to preselected mutual chromophore orientations, which do not show strong enhancement/suppression effects of excitonic coupling. This result, however, depends on the properties of the specific system and most likely does not hold in general.

Recently, it was found¹² that the TIP3P parameterization of water molecules in combination with AMBER force field parameters of the polyproline–chromophore system leads to a bias in the statistical weight of the different conformations toward the closed conformation, in which Alexa 488 gets close to the polyproline helix and the interchromophore distances are small (shown in the right part of Figure 2). To remove this bias, the authors propose to combine the AMBER force field with a scaled TIP4P water model, and within PDA, they obtain a FRET efficiency of 0.83 for the all-trans P11, which is also investigated in the present work. Because this value is above our PDA value (0.81) and a bias toward the closed conformation is

expected to increase the FRET efficiency, due to the smaller interchromophore distances, it seems that our force field combination (CHARMM-TIP3P) does not contain such a bias. More direct support for this conclusion is obtained by investigating the contact between Alexa 488 and polyproline in detail. The closest distance between this chromophore and the polyproline helix is shown in Figure 9 for some selected trajectories for P11, P14, and P20. Besides relatively rapid fluctuations with amplitudes in the range of 3–15 Å, periods of up to a few tens of ns are visible with small amplitude fluctuations around a distance of 2.5 Å. We repeated an earlier analysis¹² and determined the fraction of conformations with a closest distance smaller than 3 Å, referred to as “bound state”, where the Alexa chromophore is in a closed conformation (as depicted in Figure 2, right part). We obtain fractions of 49, 58, and 55% for P11, P14, and P20, respectively, which are at the upper limit of the 20–50% range suggested to be realistic before.¹² These bound states are important contributors to the static disorder in Figure 8.

For static disorder, we consider all fluctuations that are slower than the excited state lifetime of the isolated chromophores (4 ns). We made use of this separation between static and dynamic disorder in the averages of the efficiencies and rate constants in eq 22. The border between slow and fast disorder is somewhat weakly defined because the excited state lifetime of the isolated chromophores represents only an upper bound for the actual excited state lifetime of the donor in the coupled system. Excitation energy transfer, in particular for short distances, leads to shorter lifetimes. To investigate whether our procedure suffers from such a systematic error, we have performed MC calculations. The efficiencies obtained by these MC calculations are practically identical to the efficiencies obtained from the averaged rate constants for all helix lengths. The deviations in the 0.01 efficiency unit range are below the minimal experimental uncertainty in single-molecule experiments.¹³ In particular, the deviations do not depend on the interchromophore distance. Hence, the above described systematic error is small.

A subtlety in the interpretation of the experimental data on the present polyproline system concerns the influence of a small fraction of systems with a single proline in cis conformation. It would be helpful to also measure, besides the FRET efficiency of P20,³⁷ the remaining helices P6, P11, and P14 in TFE solution, where no internal cis conformations occur, in order to check the present estimates for the changes in efficiency ΔE_N (eq 29) that are based on Förster theory.

CONCLUSIONS

In the present work, we have extended the analysis of FRET experiments to short interchromophore distances. The new method, which combines all-atom MD simulations with quantum chemical/electrostatic calculations of the excitonic coupling goes beyond the PDA, takes into account microscopic information about the conformational substates of the system, and includes a microscopic model for screening and local field correction effects in the excitonic coupling. This method was successfully applied to a polyproline helix of variable length labeled with Alexa dyes, revealing quantitative agreement with mean average FRET efficiencies from single-molecule experiments. In particular, the deviations of experimental efficiencies from predictions of the standard Förster theory, observed for short and intermediate helix lengths, are explained in detail. We find that for the present system, the neglect of static disorder in

interchromophore distances and orientations is responsible for the overestimation of the FRET efficiency by the Förster theory. In the case of intermediate helix lengths, Förster theory, due to a fortuitous error compensation between different approximations, is still able to infer qualitatively correct interchromophore distances, whereas for the shortest helix P6, the distance predicted by Förster theory is about 30% too large. Error compensation effects in the conformational average lead to excellent performance of the PDA in the calculation of the FRET efficiency for P6. Therefore, not the PDA but the additional approximations in Förster theory, discussed above, are responsible for the overestimation of the intermolecular distance for P6.

The quantitatively correct MD/Poisson-TrEsp method can be further simplified by approximating the local field and screening effects by an effective dielectric constant, which, however, has to be determined by comparison of Poisson-TrEsp and TrEsp couplings obtained for a subset of molecular conformations. For the present system, excellent quantitative agreement between TrEsp and Poisson-TrEsp FRET efficiencies was obtained by introducing a single effective dielectric constant, independent of interchromophore distance and orientation. The MD/Poisson-TrEsp and MD/TrEsp methods introduced in the present work can be expected to be very helpful in the quantitative interpretation of FRET experiments on other biomolecules in the future, because these methods are numerically efficient and accurate at all intermolecular distances. They can be the theoretical counterpart to the recently established experimental protocol for high precision single-molecule FRET experiments.¹³

ASSOCIATED CONTENT

Supporting Information

The Supporting Information is available free of charge on the ACS Publications website at DOI: 10.1021/acs.jpcc.7b09535.

Structure of chromophores and atomic transition charges of the chromophores (PDF)

CHARMM parameter file of the force field (TXT)

CHARMM topology file of the force field (TXT)

AUTHOR INFORMATION

Corresponding Author

*E-mail: thomas.renger@jku.at.

ORCID

Thomas Renger: 0000-0001-9245-3805

Notes

The authors declare no competing financial interest.

ACKNOWLEDGMENTS

This work was supported by the Doctorate College program “Nano-Analytics of Cellular Systems (NanoCell)” of the Austrian Science Fund (FWF) (grant number: W 1250).

REFERENCES

- (1) Förster, Th. Zwischenmolekulare Energiewanderung und Fluoreszenz. *Ann. Phys.* **1948**, *437*, 55–75.
- (2) Stryer, L.; Haugland, R. P. Energy Transfer: A Spectroscopic Ruler. *Proc. Natl. Acad. Sci. U.S.A.* **1967**, *58*, 719–726.
- (3) Schuler, B. Single-Molecule Fluorescence Spectroscopy of Protein Folding. *ChemPhysChem* **2005**, *6*, 1206–1220.

- (4) Watkins, L. P.; Chang, H.; Yang, H. Quantitative Single-Molecule Conformational Distributions: A Case Study with Poly-(L-Proline). *J. Phys. Chem. A* **2006**, *110*, 5191–5203.
- (5) Schuler, B.; Eaton, W. A. Protein Folding Studied by Single-Molecule FRET. *Curr. Opin. Struct. Biol.* **2008**, *18*, 16–26.
- (6) Li, P. T.; Vieregg, J.; Tinoco, I. How RNA Unfolds and Refolds. *Annu. Rev. Biochem.* **2008**, *77*, 77–100.
- (7) Joo, C.; Balci, H.; Ishitsuka, Y.; Buranachai, C.; Ha, T. Advances in Single-Molecule Fluorescence Methods for Molecular Biology. *Annu. Rev. Biochem.* **2008**, *77*, 51–76.
- (8) Brucalé, M.; Schuler, B.; Samori, B. Single-Molecule Studies of Intrinsically Disordered Proteins. *Chem. Rev.* **2014**, *114*, 3281–3317.
- (9) Chung, H. S.; Meng, F.; Kim, J.-Y.; McHale, K.; Gopich, I. V.; Louis, J. M. Oligomerization of the Tetramerization Domain of P53 Probed by Two- and Three-Color Single-Molecule FRET. *Proc. Natl. Acad. Sci. U.S.A.* **2017**, *114*, E6812–E6821.
- (10) Hoefling, M.; Lima, N.; Haenni, D.; Seidel, C. A. M.; Schuler, B.; Grubmüller, H. Structural Heterogeneity and Quantitative FRET Efficiency Distributions of Polyprolines Through a Hybrid Atomistic Simulation and Monte Carlo Approach. *PLoS One* **2011**, *6*, No. e19791.
- (11) Chung, H. S.; Gopich, I. V. Fast Single-Molecule FRET Spectroscopy: Theory and Experiment. *Phys. Chem. Chem. Phys.* **2014**, *16*, 18644–18657.
- (12) Best, R. B.; Hofmann, H.; Nettels, D.; Schuler, B. Quantitative Interpretation of FRET Experiments via Molecular Simulation: Force Field and Validation. *Biophys. J.* **2015**, *108*, 2721–2731.
- (13) Hellenkamp, B.; Schmid, S.; Doroshenko, O.; Opanasyuk, O.; Kühnemuth, R.; Adariani, S. R.; Barth, A.; Birkedal, V.; Bowen, M. E.; Chen, H.; et al. Precision and Accuracy of Single-Molecule FRET Measurements - a Worldwide Benchmark Study. 2017, arXiv:1710.03807. arXiv.org e-Print archive. <https://arxiv.org/abs/1710.03807>.
- (14) Schuler, B.; Lipman, E. A.; Steinbach, P. J.; Kumke, M.; Eaton, W. A. Polyproline and the “Spectroscopic Ruler” Revisited with Single-Molecule Fluorescence. *Proc. Natl. Acad. Sci. U.S.A.* **2005**, *102*, 2754–2759.
- (15) Scholes, G. D. Long-Range Resonance Energy Transfer in Molecular Systems. *Annu. Rev. Phys. Chem.* **2003**, *54*, 57–87.
- (16) Beljonne, D.; Curutchet, C.; Scholes, G. D.; Silbey, R. J. Beyond Förster Resonance Energy Transfer in Biological and Nanoscale Systems. *J. Phys. Chem. B* **2009**, *113*, 6583–6599.
- (17) Olaya-Castro, A.; Scholes, G. D. Energy Transfer from Förster-Dexter Theory to Quantum Coherent Light-Harvesting. *Int. Rev. Phys. Chem.* **2011**, *30*, 49–77.
- (18) Krueger, B. P.; Scholes, G. D.; Fleming, G. R. Calculation of Couplings and Energy-Transfer Pathways between the Pigments of LH2 by the ab initio Transition Density Cube Method. *J. Phys. Chem. B* **1998**, *102*, 5378–5386.
- (19) Scholes, G. D.; Gould, I. R.; Cogdell, R. J.; Fleming, G. R. Ab initio Molecular Orbital Calculations of Electronic Couplings in the LH2 Bacterial Light-Harvesting Complex of Rps. acidophila. *J. Phys. Chem. B* **1999**, *103*, 2543–2553.
- (20) Fink, R. F.; Pfister, J.; Schneider, A.; Zhao, H.; Engels, B. Ab initio Configuration Interaction Description of Excitation Energy Transfer Between Closely Packed Molecules. *Chem. Phys.* **2008**, *343*, 353–361.
- (21) Beenken, W. J. D.; Pullerits, T. Excitonic Coupling in Polythiophenes: Comparison of Different Calculation Methods. *J. Chem. Phys.* **2004**, *120*, 2490–2495.
- (22) Wong, K. F.; Bagchi, B.; Rossky, P. J. Distance and Orientation Dependence of Excitation Transfer Rates in Conjugated Systems: Beyond the Förster Theory. *J. Phys. Chem. A* **2004**, *108*, 5752–5763.
- (23) Wiesenhofer, H.; Beljonne, D.; Scholes, G. D.; Hennebicq, E.; Bredas, J.-L.; Zojger, E. Limitations of the Förster Description of Singlet Exciton Migration: The Illustrative Example of Energy Transfer to Ketonic Defects in Ladder-type Poly(para-phenylenes). *Adv. Funct. Mater.* **2005**, *15*, 155–160.
- (24) Madjet, M. E.; Abdurahman, A.; Renger, T. Intermolecular Coulomb Couplings from ab initio Electrostatic Potentials: Application to Optical Transitions of Strongly Coupled Pigments in Photosynthetic Antennae and Reaction Centers. *J. Phys. Chem. B* **2006**, *110*, 17268–17281.
- (25) Schrier, J.; Wang, L.-W. Shape Dependence of Resonant Energy Transfer between Semiconductor Nanocrystals. *J. Phys. Chem. C* **2008**, *112*, 11158–11161.
- (26) Muñoz-Losa, A.; Curutchet, C.; Krueger, B. P.; Hartsell, L. R.; Mennucci, B. Fretting about FRET: Failure of the Ideal Dipole Approximation. *Biophys. J.* **2009**, *96*, 4779–4788.
- (27) Agranovich, V. M.; Galanin, M. D. *Electronic Excitation Energy Transfer in Condensed Matter*; North-Holland Publishing Company: Amsterdam, The Netherlands, 1982.
- (28) Böttcher, C. J. F. *Theory of Electric Polarization*; Elsevier: Amsterdam, The Netherlands, 1973.
- (29) Hsu, C.; Head-Gordon, M.; Head-Gordon, T.; Fleming, G. R. Excitation Energy Transfer in Condensed Media. *J. Chem. Phys.* **2001**, *114*, 3065–3072.
- (30) Renger, T.; Müh, F. Theory of Excitonic Couplings in Dielectric Media. *Photosynth. Res.* **2012**, *111*, 47–52.
- (31) Scholes, G. D.; Curutchet, C.; Mennucci, B.; Cammi, R.; Tomasi, J. How Solvent Controls Electronic Energy Transfer and Light Harvesting. *J. Phys. Chem. B* **2007**, *111*, 6978–6982.
- (32) Renger, T.; Madjet, M. E.; Schmidt am Busch, M.; Adolphs, J.; Müh, F. Structure-Based Modeling of Energy Transfer in Photosynthesis. *Photosynth. Res.* **2013**, *116*, 367–388.
- (33) Curutchet, C.; Scholes, G. D.; Mennucci, B.; Cammi, R. How Solvent Controls Electronic Energy Transfer and Light Harvesting: Toward a Quantum-Mechanical Description of Reaction Field and Screening Effects. *J. Phys. Chem. B* **2007**, *111*, 13253–13265.
- (34) Dale, R. E.; Eisinger, J.; Blumberg, W. E. The Orientational Freedom of Molecular Probes: The Orientation Factor in Intramolecular Energy Transfer. *Biophys. J.* **1979**, *26*, 161–194.
- (35) Wu, P.; Brand, L. Orientation Factor in Steady-State and Time-Resolved Resonance Energy Transfer Measurements. *Biochemistry* **1992**, *31*, 7939–7947.
- (36) Van Beek, D. B.; Zwier, M. C.; Shorb, J. M.; Krüger, B. P. Fretting about FRET: Correlation between κ and R . *Biophys. J.* **2007**, *92*, 4168–4178.
- (37) Best, R. B.; Merchant, K. A.; Gopich, I. V.; Schuler, B.; Bax, A.; Eaton, W. A. Effect of Flexibility and Cis Residues in Single-Molecule FRET Studies of Polyproline. *Proc. Natl. Acad. Sci. U.S.A.* **2007**, *104*, 18964–18969.
- (38) Adolphs, J.; Müh, F.; Madjet, M. E.; Renger, T. Calculation of Pigment Transition Energies in the FMO Protein: From Simplicity to Complexity and Back. *Photosynth. Res.* **2008**, *95*, 197–209.
- (39) Doose, S.; Neuweiler, H.; Barsch, H.; Sauer, M. Probing Polyproline Structure and Dynamics by Photoinduced Electron Transfer Provides Evidence for Deviations From a Regular Polyproline Type II Helix. *Proc. Natl. Acad. Sci. U.S.A.* **2007**, *104*, 17400–17405.
- (40) Schimmel, P. R.; Flory, P. J. Conformational Energy and Configurational Statistics of Poly-L-Proline. *Proc. Natl. Acad. Sci. U.S.A.* **1967**, *58*, 52–59.
- (41) May, V.; Kühn, O. *Charge and Energy Transfer Dynamics in Molecular Systems: A Theoretical Introduction*; Wiley-VCH: Berlin, 2000.
- (42) MacKerell, A. D.; Bashford, D.; Bellott, M.; Dunbrack, R. L.; Evanseck, J. D.; Field, M. J.; Fischer, S.; Gao, J.; Guo, H.; Ha, S.; et al. All-Atom Empirical Potential for Molecular Modeling and Dynamics Studies of Proteins. *J. Phys. Chem. B* **1998**, *102*, 3586–3616.
- (43) Brooks, B. R.; Brooks, C. L., III; Mackerell, A. D., Jr.; Nilsson, L.; Petrella, R. J.; Roux, B.; Won, Y.; Archontis, G.; Bartels, C.; Boresch, S.; et al. CHARMM: The Biomolecular Simulation Program. *J. Comput. Chem.* **2009**, *30*, 1545–1614.
- (44) Jorgensen, W. L.; Chandrasekhar, J.; Madura, J. D. Comparison of Simple Potential Functions for Simulating Liquid Water. *J. Chem. Phys.* **1983**, *79*, 926–935.

(45) Phillips, J. C.; Braun, R.; Wang, W.; Gumbart, J.; Tajkhorshid, E.; Villa, E.; Chipot, C.; Skeel, R. D.; Kale, L.; Schulten, K. Scalable Molecular Dynamics with NAMD. *J. Comput. Chem.* **2005**, *26*, 1781–1802.

(46) Bochevarov, A. D.; Harder, E.; Hughes, T. F.; Greenwood, J. R.; Braden, D. A.; Philipp, D. M.; Rinaldo, D.; Halls, M. D.; Zhang, J.; Friesner, R. A. Jaguar: A High-Performance Quantum Chemistry Software Program with Strengths in Life and Materials Sciences. *Int. J. Quantum Chem.* **2013**, *113*, 2110–2142.

(47) Shao, Y.; Molnar, L. F.; Jung, Y.; Kussmann, J.; Ochsenfeld, C.; Brown, S. T.; Gilbert, A. T. B.; Slipchenko, L. V.; Levchenko, S. V.; O'Neill, D. P.; et al. Advances in Methods and Algorithms in a Modern Quantum Chemistry Program Package. *Phys. Chem. Chem. Phys.* **2006**, *8*, 3172–3191.

(48) Sigfridsson, E.; Ryde, U. Comparison of Methods for Deriving Atomic Charges from the Electrostatic Potential and Moments. *J. Comput. Chem.* **1998**, *19*, 377–395.

(49) Bashford, D. In *Scientific Computing in Object-Oriented Parallel Environments*; Ishikawa, Y., Oldehoeft, R. R., Reynders, J. V. W., Tholburn, M., Eds.; Springer: Berlin, 1997; pp 233–240.